NASA TN D-1321

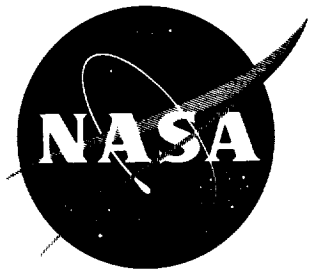

TECHNICAL NOTE

D-1321

EXPERIMENTAL PERFORMANCE OF AN ION ROCKET ENGINE USING A RECTANGULAR-SLAB POROUS-TUNGSTEN EMITTER

By Ronald J. Cybulski, Joseph T. Kotnik,
and David L. Lockwood

Lewis Research Center
Cleveland, Ohio

NATIONAL AERONAUTICS AND SPACE ADMINISTRATION

WASHINGTON November 1962

NATIONAL AERONAUTICS AND SPACE ADMINISTRATION

TECHNICAL NOTE D-1321

EXPERIMENTAL PERFORMANCE OF AN ION ROCKET ENGINE USING A RECTANGULAR-SLAB POROUS-TUNGSTEN EMITTER

By Ronald J. Cybulski, Joseph T. Kotnik,
and David L. Lockwood

SUMMARY

An ion rocket engine employing a 0.3- by 6-inch porous-tungsten ionizer has been successfully operated. The ionizer was constructed entirely from refractory metals. An electron-beam weld and a high-temperature-furnace braze were used to assemble the parts. During a total of more than 50 hours of test operations, no structural failures occurred with this arrangement.

Accelerator and power efficiencies up to 90 and 70 percent, respectively, at current densities up to 113 amperes per square meter were obtained. The aforementioned power efficiency was obtained at a specific impulse of 8680 seconds. Experimentally measured values of power efficiency for various types of ion-beam sources are compared.

An experimentally measured value of propellant utilization of approximately 90 percent is reported. A direct comparison is made between metered data and data from a conventional calorimeter.

INTRODUCTION

This program was undertaken to investigate a 0.3- by 6-inch porous-tungsten ionizer. An ionizer of this size is desirable for two reasons: First, since it is desirable to have an ion rocket with high thrust density, it is necessary to keep the ionizer surface as large as possible in comparison with the total frontal area. Second, since it is necessary to maintain a high power efficiency, the current density should be kept as high as possible and the ionizer heat losses should be kept as low as possible. With these requirements as goals, fabrication of a porous-tungsten ionizer was undertaken.

One of the major problems connected with the use of a porous-tungsten ionizer has been fabricating the ionizer. Leaks in the mounting joints must be much smaller than the pores of the ionizer; otherwise, serious inefficiencies will result. This poses serious joining problems for two reasons: (1) The high work function of the porous tungsten must be preserved, and (2) no weld material can be allowed to run over the ionizer surface, since this would result in filling or blocking of the pores. The materials used for joining should have low vapor pressures so that evaporation of the weld material will not create local high-pressure regions and as a result affect operating voltages in the engine. The ionizers must be operated at temperatures in excess of 1370° K without further sintering of the material and must withstand temperature cycling.

Many techniques for joining porous tungsten have been tried; among these are brazing with various materials, resistance welding, arc welding, arc spraying, and electron-beam welding. These techniques are discussed in reference 1.

Several sizes and shapes of porous-tungsten ionizers have been tried. One type (ref. 2) used 1/4-inch-diameter porous-tungsten plugs. Another type (ref. 3) employed a porous-tungsten annular ring with a mean diameter of 3 inches.

The porous ionizer to be discussed herein is in the form of a slab, 0.3 inch wide and 6 inches long, and was fabricated from refractory metals. The technique used to join these metals was electron-beam welding. This method, together with the performance of an ion rocket engine using the ionizer, is described in this report.

APPARATUS AND ENGINE DESIGN

Facility

Vacuum chamber. - The data reported herein were obtained from experiments conducted in one of the high-vacuum electric-rocket research facilities at the Lewis Research Center. Figure 1 shows a cutaway of the vacuum facility with the engine installed. The engine was mounted on an aluminum end plate (see fig. 2), which was inserted into a 14-inch-long metal bell jar. The engine chamber is separated from the main portion of the vacuum facility by a 12-inch-diameter, pneumatically operated gate valve. Adjustments and changes in the engine could be made quickly and conveniently if the valve between the bell jar and tank was closed; thus the vacuum in the tank could be maintained continuously. A 3.28-foot-long section of the 5-foot-diameter tank housed the conventional calorimeters. The remainder of the tank contained the liquid-nitrogen-cooled condenser baffles, which were used to condense the cesium ejected from the engine. The pressure in the engine chamber and main portion of

the facility was maintained in the low 10^{-6} torr range while the engine was operating, except at high flow rates of cesium that correspond to current densities in excess of 100 amperes per square meter. At the high flow rates the pressure maintained in the facility while the engine was operating was in the high 10^{-6} torr range.

Ion engine. - The engine (fig. 2) was a modified version of the porous-tungsten - cesium ion engine of reference 4. The disassembled engine is shown in figure 3(a).

Cesium propellant is contained in a stainless-steel vaporizer located behind the porous-tungsten ionizer. The cesium vapor passes through a 1/4-inch-diameter tantalum tube, which is flanged to a 1/8-inch-diameter tantalum tube, into a reservoir behind the ionizer. The cesium vapor then passes through the porous tungsten and is ionized. Cesium ions created at the ionizer are accelerated by an electrostatic field maintained between the ionizer and the accelerator electrode. A beam-forming electrode maintained at the same potential as the ionizer is located at the downstream surface of the ionizer. Its purpose is to contain the ion beam within the prescribed boundaries. The accelerator electrode is maintained at a negative potential equal to or less than 3 kilovolts to prevent backstreaming of electrons.

The schematic shown in figure 3(b) gives the location of the power supplies and current meters used to monitor engine performance. All electrical leads, thermocouples, and air-cooling connections are brought through aluminum oxide standoffs mounted on the end plate (see fig. 2). An engine isolation screen maintained at a negative 300 volts is located just downstream of the accelerator electrode. The screen prevents secondary electrons created in the test environment from reaching the engine. Such an electron flow would cause the ground return meter to indicate erroneously high beam currents.

Instruments

Electrical meters. - All the meters used in this research were conventional commercial meters with an estimated maximum error of ±3 percent. Multiple shunt circuits were used with the meters to allow for accurate readings over a wide range of values. Net ion-beam powers, accelerator-power losses, power input to the ionizer, and vaporizer powers were calculated from the observed meter readings.

Conventional calorimeter. - A complete discussion of the development of the calorimeter can be found in reference 4. This device converts the ion-beam kinetic energy to heat at a square copper collector plate. The heat flows by conduction through a thermal-resistance can to reach the heat sink, which consists of a rapidly flowing stream of water in the 1/4-inch copper tubing. Since the flow of heat is essentially one-dimensional, the beam power can be calculated if the steady-state

temperature drop is measured. A vertical array of five such units, each 2 inches square, was attached to an actuator device, which moved it across the facility in a direction normal to the beam. The measured readings at each position were summed up and compared with the total power obtained from the meter readings.

Vaporizer Design

The vaporizer was constructed of stainless steel and was cylindrical in shape, 2 inches in diameter, and 4.38 inches long. The removable top facilitated the loading of the glass ampules that contained the cesium propellant; the ampules were broken manually from the outside by a rod-and-bellows assembly. A 1/4-inch valve was included in the vaporizer so that it could be evacuated before the ampules were broken. Evacuation of the vaporizer was deemed necessary to prevent contamination of the cesium upon exposure to the vaporizer's atmosphere. The vaporizer was heated with a resistance heater and cooled by air, which passed through a tube coiled around the vaporizer. An iron-constantan thermocouple, located at the coldest portion of the vaporizer, was used to monitor propellant flow rate, which is a function of vaporizer temperature.

Ionizer Design

An initial attempt (see ref. 4) to use a porous-tungsten ionizer held in place by a mechanical clamping arrangement proved undesirable because of both the excessive conduction heat losses through the beam-forming electrode and the leakage of propellant around the ionizer. The power input required to heat the ionizer was 1.29×10^6 watts per square meter at 1370° K. Subsequently, an attempt was made to design an ionizer that met the following requirements:

(1) Simplicity of design

(2) Freedom from leaks around the porous ionizer

(3) Durability

(4) High heating efficiency

Electron-beam welding was used to bond the porous ionizer to its support. The technique is described in appendix B.

The first successful ionizer using this technique is shown in figure 4. It consisted of a 0.3- by 6- by 0.05-inch porous-tungsten strip, which was electron-beam-welded into a 2- by 8-inch tungsten frame. This frame was then brazed to the flanges of a 1- by 1.25- by 6-inch

tantalum box into which cesium was allowed to flow. This design met the first three requirements previously mentioned, but the power required to heat the ionizer was relatively high (viz., 5.17×10^5 w/sq m at 1370° K). This number can be compared with the total hemispherical black-body radiation at 1370° K of 1.9×10^5 watts per square meter. For this reason, a second design was conceived.

The second unit consisted of a 0.3- by 6- by 0.05-inch porous-tungsten ionizer electron-beam-welded to a 6- by 0.01-inch tungsten channel. This arrangement is shown in figure 3(a). The ends of the channel were brazed until they were closed. The propellant supply tube entered from the end of the channel. The porous ionizer was heated by radiation and conduction from the back wall of the channel, which was heated by radiation from a 0.005- by 0.31- by 6-inch tantalum heater filament. The power required was 1.51×10^5 watts per square meter at 1370° K.

The ionizer channel was mounted inside a five-sided box to facilitate heat shielding. The function of the box was to add structural rigidity to the channel and to hold the heat shielding in place. Connections for engine mounting were made at points where the temperature was low; thus conduction losses were minimized. The engine could be removed from the vacuum facility if the four bolts that held the aluminum end plate to the metal bell jar were taken out.

Electrode Design

Since a complete description of the electrode design procedure is presented in reference 4, it is only briefly summarized herein. The Poisson equation is solved to obtain the potential distribution along the edge of an ion beam having the desired shape. This potential distribution and the boundary condition of zero electric field strength normal to the edge of the beam can be used to solve the Laplace equation in the charge-free region outside the beam. This solution determines the equipotential shapes outside the desired beam. Metal electrodes, which conform to these equipotential shapes and are maintained at the proper voltages and distances relative to the ion source, theoretically confine the ion beam to the desired region. The use of a finite number of electrodes and the neglect of aperture effects, however, adversely affect the theoretical confinement.

RESULTS AND DISCUSSION

Propellant Utilization Efficiency

A test was run for a fixed period of time at constant operating conditions with the ionizer and propellant feed system to measure the

propellant utilization efficiency η_u. (Symbols are defined in appendix A.) The amount of cesium remaining after the test run was determined by chemical analysis. Subtracting this from the original amount of cesium and dividing the difference by the run time yield the average mass-flow rate. Converting this value of mass-flow rate into its equivalent current and dividing it into the ion current delivered by the engine produce an estimate of η_u. The experimental value obtained in this manner was $\eta_u \approx 90 \pm 3$ percent. Two possible reasons for error present in this method are: (1) All the unused propellant might not have been removed from the vaporizer and feed system before the chemical analysis, and (2) there could have been a very small leak in the propellant feed system. The problem of intermittent leaks in the flange connecting the ionizer assembly to the vaporizer has been observed since the construction of the leak-tight ionizer, and several methods of sealing the system are presently being investigated. Both of these problems could make the observed value of propellant utilization efficiency lower than the actual value.

Ionizer Power Consumption

The major energy loss in an ion rocket engine is the power required to heat the ionizer. Therefore, independent heat-shielding tests were conducted to determine the effect of various combinations of heat shielding on the reduction of power input to the ionizer as read on conventional meters.

In these heat-shielding tests, the ionizer was mounted in a manner similar to but not the same as that used in the actual engine. In addition, the beam-forming and accelerator electrodes were not present. Figure 5 compares the various heat-shielding plans. The power input to the ionizer, as indicated by conventional meters, is shown as a function of the observed ionizer temperature. Initially, the ionizer was operated without tantalum heat shielding, and the necessary data were obtained. Then a single heat shield was placed around the three sides of the channel, and the run was repeated. Multiple heat shields (viz., 6, 16, and 27) were tested. Because the power consumption was approximately the same for 6, 16, and 27 heat shields, only data for the 27 heat shields are shown. The final run represented occurred with the 27 heat shields and a strip of Fiberfrax insulation placed between the edge of the channel and the first heat shield. The power required for this configuration was 2.93×10^5 watts per square meter at 1370° K. The bottom curve represents the actual heat-shielding configuration used to obtain the engine-performance data presented herein. The major part of the difference in power input between the bottom curve and the one above it, other than the difference in conduction heat losses from the two mounting arrangements, can be attributed to the effectiveness of the accelerator electrodes as heat shields. In fact, it was determined experimentally

that, of the 170-watt difference in power between these curves at 1370° K, 30 watts can be charged to conduction heat losses and the remaining 140 watts to heat-shielding effects of the electrodes. Therefore, the ratio of power with electrodes to power without electrodes for an acceleration length-width-ratio of 1 is numerically equal to 0.55. If the electrodes served as perfect heat shields, this value would be 0.41, as indicated in reference 5. These data show that the electrodes do serve as reasonably good heat shields. The resultant power that was used to heat the ionizer to 1370° K with the complete engine assembly is 1.51×10^{5} watts per square meter.

Conventional Calorimeter

It had previously been shown (ref. 4) that electrons backstreaming to the engine result in the meters showing a higher beam current than that which actually existed. As an independent check, however, the conventional calorimeter was used to monitor ion-beam power in conjunction with the metering. Figure 6 shows a typical data map for a given engine setting, namely, 59 milliamperes of beam current at a net acceleration voltage of 5 kilovolts. From the power that each 25.8-square-centimeter area received, a total power of 229.61 watts was obtained. The power computed from the engine meters was 295 watts. This represented agreement to within 23 percent. The disagreement may have been caused by two effects:

(1) The ion beam diverged, and a fraction of the ion beam current impinged on the orifice screen. This resulted in a loss of power, since the calorimeter was located downstream of the screen. The magnitude of the ion current lost to the screen cannot be determined accurately because of the effect of secondary electron emission. (The screen is necessary, however, to suppress secondary electron emission from the orifice baffle.)

(2) A numerical value of less than unity for the accommodation coefficient would have resulted in the data falling below the metered power; thus, metered power in general is higher than probe power. This fact is also substantiated in reference 6.

Ion-Beam Current Density

This section and the following three sections deal with engine performance. Beam, accelerator, and radiation power are all based on electrical measurements.

Figure 7 compares the current densities obtained experimentally to those calculated from Child's law for space-charge-limited flow as a

function of acceleration potential for an acceleration distance of 0.30 inch. Below the saturation region, these data fall reasonably close to Child's law.

Two reasons for the observed divergence of the data from Child's law before saturation are as follows:

(1) Nonuniform work function. Any emitter can exhibit small variations in work function over its surface so that some portions reach saturation at lower values of potential than others. This results in a rounding off of the curve, as demonstrated in the data of figure 7.

(2) Nonuniform emitter temperature. In operation the emitter temperature is not uniform because the ends are cooled by conduction. Since the cooler portions reach emission saturation before the hotter portions do, there is a progressive deviation from the theoretical space-charge line in the region where saturation is approached.

The engine was operated at current densities as high as 113 amperes per square meter for periods of time up to 10 minutes and at current densities up to 80 amperes per square meter for periods up to $1\frac{1}{2}$ hours with no major difficulties. The run time was limited because the facility pressure, which increased with time, caused arcing between the electrodes and subsequent engine breakdowns.

Porosity of Porous Emitter

The porous-tungsten ionizers used in this program were obtained from the Semicon Associates Co. They were in the form of slabs that measured 0.3 by 6 by 0.05-inch. Cold-flow tests indicated a transmission coefficient of 4.5×10^{-5}. The transmission coefficient is defined as the ratio of arrival rate at the downstream surface to the arrival rate at the upstream surface. Figure 8 shows a photomicrograph of a portion of this porous ionizer. The average pore size of the ionizer as measured from the photomicrograph is 2.5 to 3 microns. Reference 7 discusses the theory of atom loss from a porous-tungsten ionizer as a function of pore size and ionizer temperature. When the theory in reference 7 is used for an ionizer temperature of 1500° K (approximately the range operated) and the total loss of neutral atoms from both the surface-diffusion and the vapor-phase flow is summed, a total loss of 3 to 4 percent is obtained. This value compares reasonably well with the propellant utilization efficiency of 90 percent mentioned earlier.

Accelerator Efficiency

One of the most important parameters in ion-engine operation is the accelerator efficiency η_{acc}. The accelerator efficiency is defined as the ratio of the beam power to the sum of the beam power and the power intercepted at the accelerator electrode. The efficiency may be misleading, since the electrode erosion resulting from impingement is more serious than the power loss. If an ion engine is to be of use for long-term operation, the ion impingement must be so low that the accelerator efficiency is essentially 100 percent.

For the data reported herein η_{acc} varied from 80 to 97 percent. Several factors may have contributed to these rather high impingement currents: First, the longitudinal weld between the channel and the porous-tungsten ionizer caused the unit to warp longitudinally so that the center of the ionizer was 1/16 inch away from the beam-forming electrode (sketch (a)). This warping could result in poor focusing of the

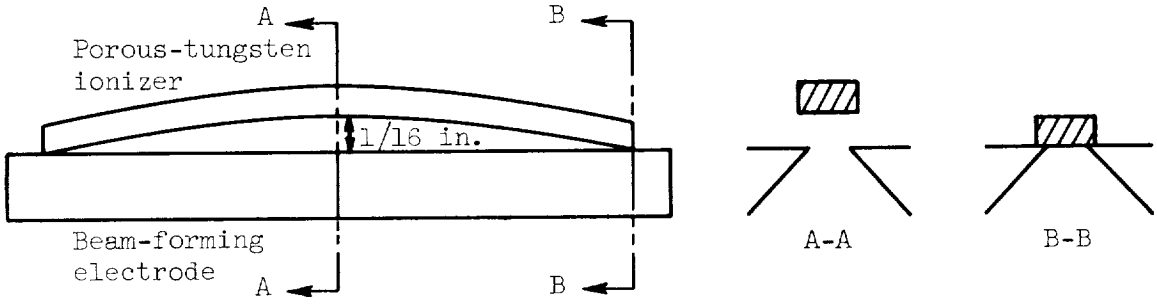

(a)

ion beam. Second, the ionizer width could not be accurately controlled and was found to be 5 percent wider than the accelerator aperture. Third, and perhaps most important, there was defocusing caused by the electric field at the accelerator aperture. A scale model of the accelerator was tested on resistance paper, and the results are shown in sketch (b). It is seen that the flux line, which intercepts the ionizer

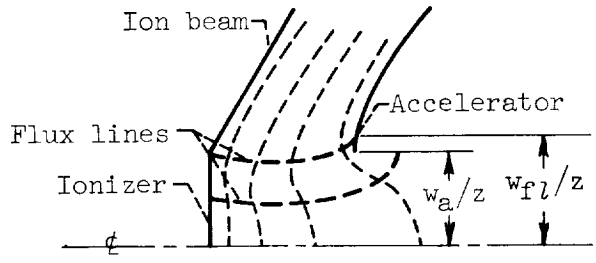

(b)

at the beam edge also intercepts the accelerator electrode. If it is assumed that the spreading of ion-flux lines is of the same order of magnitude as the ion-beam spreading, the accelerator efficiency can be estimated from the ratio of accelerator aperture width w_a to the distance between bounding flux lines at the accelerator w_{fl}. For the accelerator system used, the estimated accelerator impingement current was of the order of 5 percent. The observed accelerator impingement currents are readily explained by an accumulation of the effects just discussed.

Power Efficiency

Figure 9 shows a plot of power efficiency η_P as a function of specific impulse I at two current densities. The lower curve, which is for a current density of 40 amperes per square meter, has power efficiency up to 46 percent at a specific impulse of 7800 seconds. This efficiency corresponds to an energy requirement of 4700 electron volts per ion. The upper data point obtained at a current density of 113 amperes per square meter shows a power efficiency of 70 percent at a specific impulse of 8680 seconds and an energy requirement of 2000 electron volts per ion. For this point 5 percent of the ionizer current impinged on the accelerator electrode. If it is assumed that the impingement current can be eliminated, a power efficiency of 76 percent is obtained. This value is indicated by the solid symbol.

Figure 10 compares the performance of an electron-bombardment ion engine (ref. 8), an annular-porous-tungsten engine (ref. 3), a small-diameter-button porous-tungsten engine (ref. 2), and the porous-tungsten engine reported herein. For the purposes of this comparison two slightly different parameters are introduced. These are effective specific impulse I_{eff} and rocket efficiency η_R, as derived in reference 5. The effective specific impulse is defined as the product of the specific impulse and the propellant utilization efficiency. The rocket efficiency is defined as the product of the power efficiency and the propellant utilization efficiency.

These data indicate that, for effective specific impulses of less than 8000 seconds, the electron-bombardment engine is superior to the ion rocket engine discussed in this report. It is likely to remain superior until current densities of the order of 200 amperes per square meter are obtained or the amount of heat lost to the ionizer is further reduced.

The upper curve in figure 10, derived in reference 5 for an emissivity based on polished tungsten, depicts the theoretical values of rocket efficiency that should be obtainable for a perfectly heat shielded, rectangular-cross-section, contact-ionization engine at a

current density of 200 amperes per square meter. Whether such values can be achieved in practice remains to be determined.

SUMMARY OF RESULTS

A porous-tungsten ion engine has been operated at current densities as high as 113 amperes per square meter. The following results were obtained:

1. Power efficiencies up to 70 percent were obtained at a specific impulse of 8680 seconds. The ion current intercepted at the accelerating electrode was 5 percent of the ionizer current for this data point.

2. Electron-beam welding shows great promise for ion-rocket application. It leads to a simpler, more compact design and eliminates propellant leaks from the joints around the ionizer. It also provides a weld material that will not diffuse into the porous ionizer and thus block the pores.

3. An experimental value for propellant utilization efficiency of about 90 percent was obtained. This value could be a few percent low if all of the unused propellant were not removed from the vaporizer prior to the chemical analysis.

4. It has been demonstrated that with proper heat shielding and engine design the major sources of power loss from the engine can be greatly reduced. Power inputs as low as 1.51×10^5 watts per square meter at an ionizer temperature of 1370° K have been obtained.

Lewis Research Center
National Aeronautics and Space Administration
Cleveland, Ohio, May 24, 1962

APPENDIX A

SYMBOLS

I	specific impulse, sec
I_{eff}	effective specific impulse; $I_{eff} = I\eta_u$; sec
j	ion-beam current density, amp/m^2
P	power, w
T_v	temperature of vaporizer, ^oF
x	acceleration distance, cm
η_{acc}	accelerator efficiency
η_P	power efficiency
η_R	rocket efficiency; $\eta_R = \eta_P\eta_u$
η_u	propellant utilization efficiency
φ_0	emitter potential, kv
φ_1	accelerator electrode potential, kv

APPENDIX B

EMITTER CONSTRUCTION

The initial attempt to fabricate an emitter in which porous tungsten was electron-beam-welded to solid tungsten did not prove successful. A single 0.05- by 2- by 7-inch piece of solid tungsten with a hole in the center was used to frame the 0.3- by 6- by 0.05-inch piece of porous tungsten. Thermal stresses produced cracks in the porous tungsten; therefore, a completely sealed unit could not be fabricated in this manner.

A successfully sealed unit was constructed; it had the same dimensions as the previous unit, but the frame was made of four strips of solid tungsten. A 6-inch-long strip of solid tungsten was electron-beam-welded to each side of a piece of porous tungsten. End strips, whose length was equal to the width of the welded piece, were welded across the top and bottom to complete the front of the framed porous-tungsten emitter. Careful jigging of the pieces of tungsten before welding and preheating of the jigged units to 600° F enabled fabrication of a moderately flat, well-sealed emitter. The porous tungsten in the frame was then brazed with titanium to the flanges of a tantalum emitter box to complete the assembly. The exterior dimensions of the box were 1 by 1.25 by 6 inches. The propellant feed tube entered the back wall opposite the porous tungsten. A longitudinal duct 1/2 by 3/4 inch ran the length of the box, and a heating filament was mounted inside the duct. The filament heated the duct walls, and the walls radiantly heated the porous tungsten. This design proved completely leak tight, but it was very inefficient for heating.

The construction of a leak tight, efficiently heated emitter was accomplished by use of a U-shaped channel made from 0.01-inch tungsten. A channel was formed with an inside width of 0.304 inch and a depth of 0.15 inch. The channel and porous tungsten were then jigged in the electron-beam welder to weld the long seam. A 3-milliampere electron beam at 120 kilovolts was passed perpendicular to the porous-tungsten surface over the seam at a speed of 5 inches per minute. The beam melted both solid and porous tungsten, the 0.01-inch sheet melting fastest. The unit was then placed in an electron disintegrater machine, and the slightly oversized porous-tungsten ends were burned off to exactly the length of the channels (6 in.). End pieces, which were slightly larger than the cross section of the tube, were made out of solid tungsten; holes were burned out in the centers by the electron disintegrater machine. The end pieces and the channel unit were then jigged in the electron-beam welder, and the seams between the solid-tungsten end pieces and the porous tungsten were sealed with the electron beam.

The unit was then removed from the welding jig, and a 1/8-inch-inside-diameter tantalum tube was placed in the holes in the end plates. A brazing mixture was applied to the three open seams on the end plate and around the tube joint. The braze material, which melts at 3800° F, consists of 50 percent molybdenum powder, 40 percent molybdenum boride (MoB_2), and 10 percent titanium hydride (TiH_2). The unit with the brazing mixture applied was brazed in a vacuum (at a pressure of 2 microns).

The tube on one end of the unit was crimped and closed with a heliarc weld and was used as a support for the bottom of the emitter. A flange was attached to the longer tube at the top. This tube was used as the feed tube for the cesium vapor.

REFERENCES

1. Anon.: Investigation of Ionized Gases and Acceleration Systems for Ion Propulsion. EOS Rep. 150, Apr. 1, 1958-July 1, 1960, Electro-Optical Systems, Inc., July 20, 1960.

2. Ernstene, M. P., et al.: Development of High Efficiency Cesium Ion Engines. Paper 61-83-1777, Am. Rocket Soc., Inc., 1961.

3. Etter, J. E., et al.: The Development of a Flight Test Ion Engine. Paper 61-81-1775, Am. Rocket Soc., Inc., 1961.

4. Lockwood, David L., and Cybulski, Ronald J.: Performance Evaluation of a Two-Dimensional Ion Rocket Using Through-Feed and Porous Tungsten Ionizers. NASA TN D-766, 1961.

5. Lockwood, David L., Mickelsen, William R., and Hamza, Vladimir: Analytic Space-Charge Flow and Theoretical Electrostatic Rocket Engine Performance. Paper 2400-62, Am. Rocket Soc., Inc., 1962.

6. Richley, E. A., Sandborn, V. A., Baldwin, L. V., and Dangle, E. E.: Comparative Measurements of Beam Power in Ion-Rocket Research. NASA TN D-845, 1961.

7. Reynolds, Thaine W., and Kreps, Lawrence W.: Gas Flow, Emittance, and Ion Current Capabilities of Porous Tungsten. NASA TN D-871, 1961.

8. Reader, Paul D.: Investigation of a 10-Centimeter-Diameter Electron-Bombardment Ion Rocket. NASA TN D-1163, 1962.

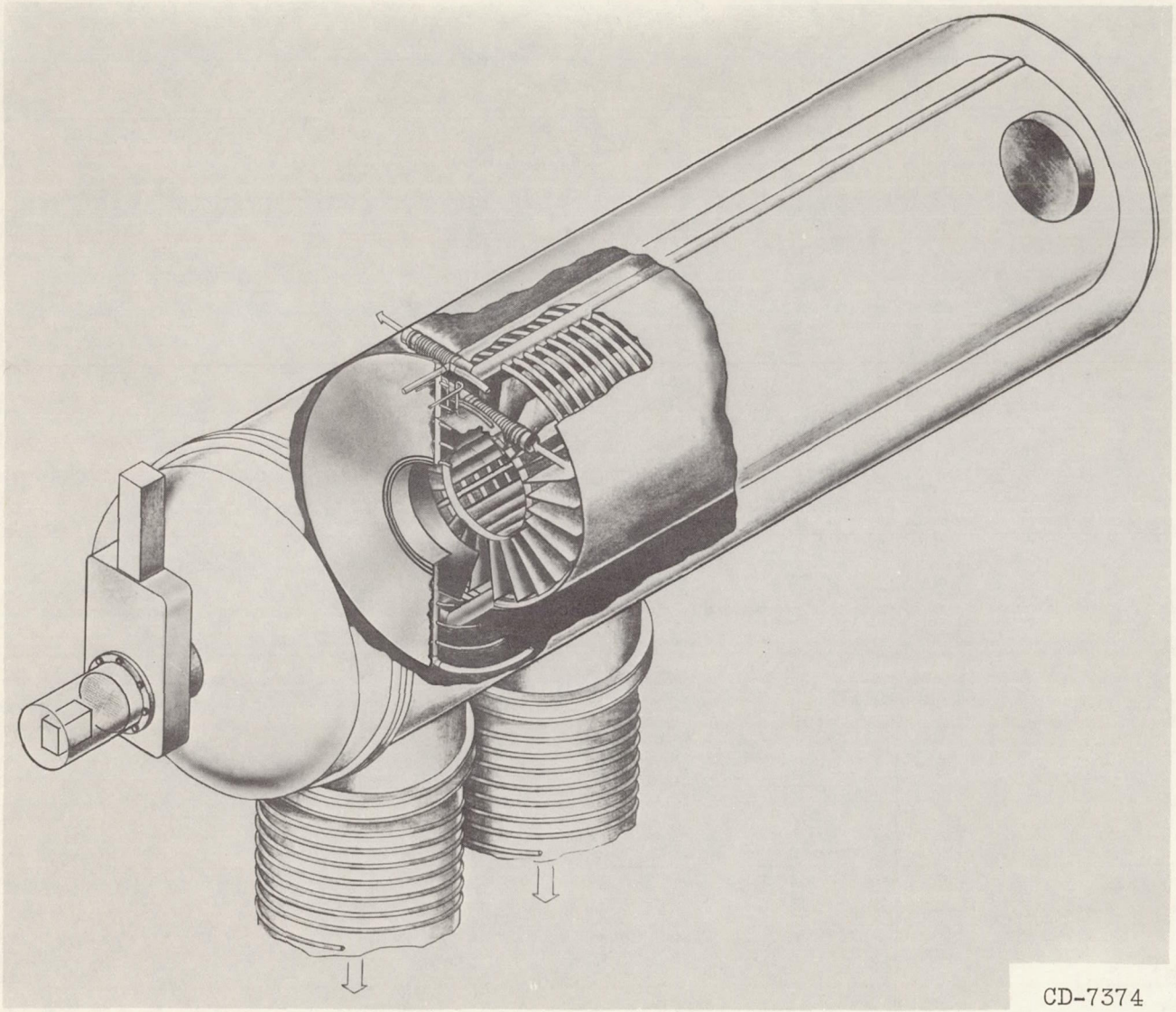

Figure 1. - Cutaway of vacuum chamber with engine installed.

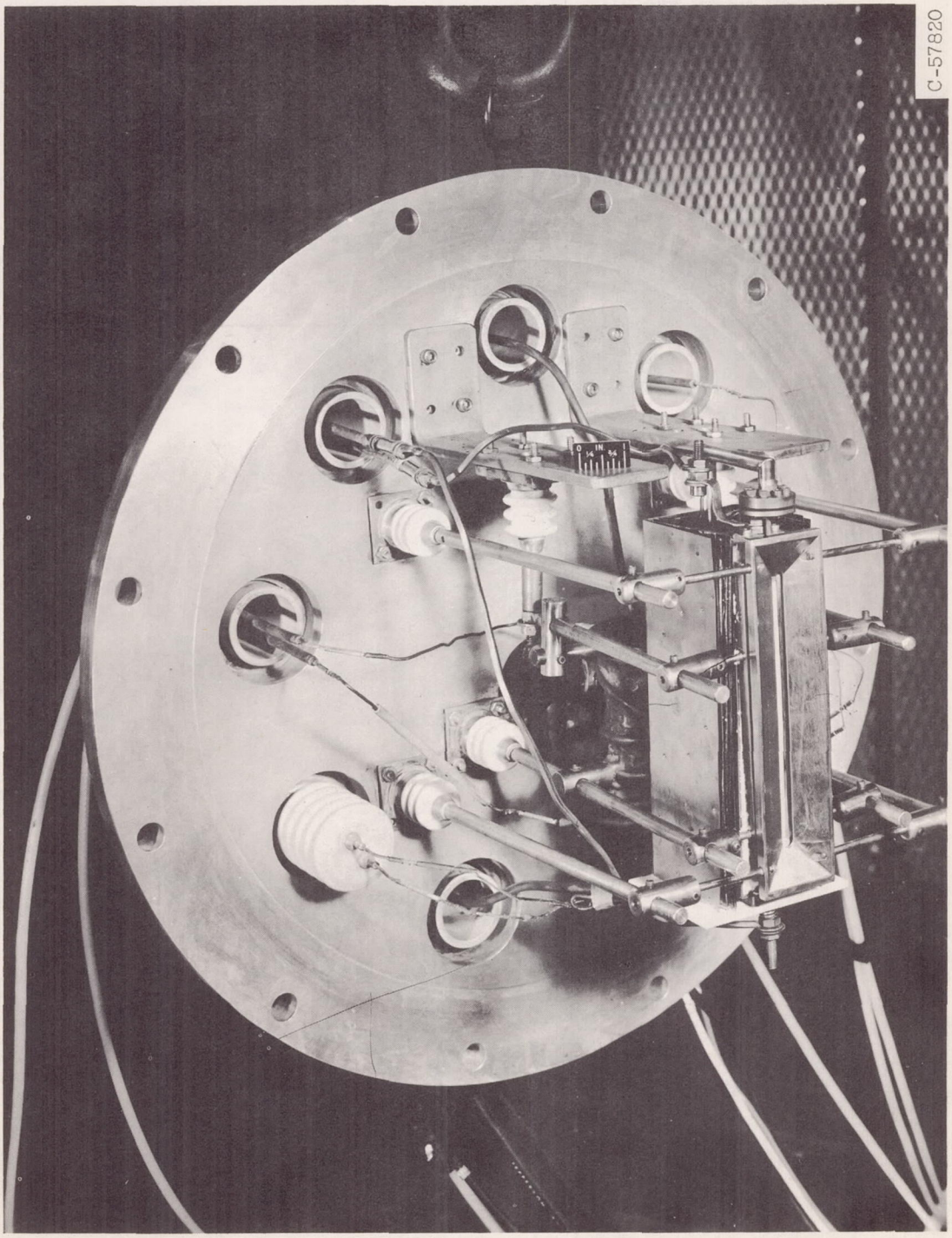

Figure 2. - Engine mounted on aluminum end plate.

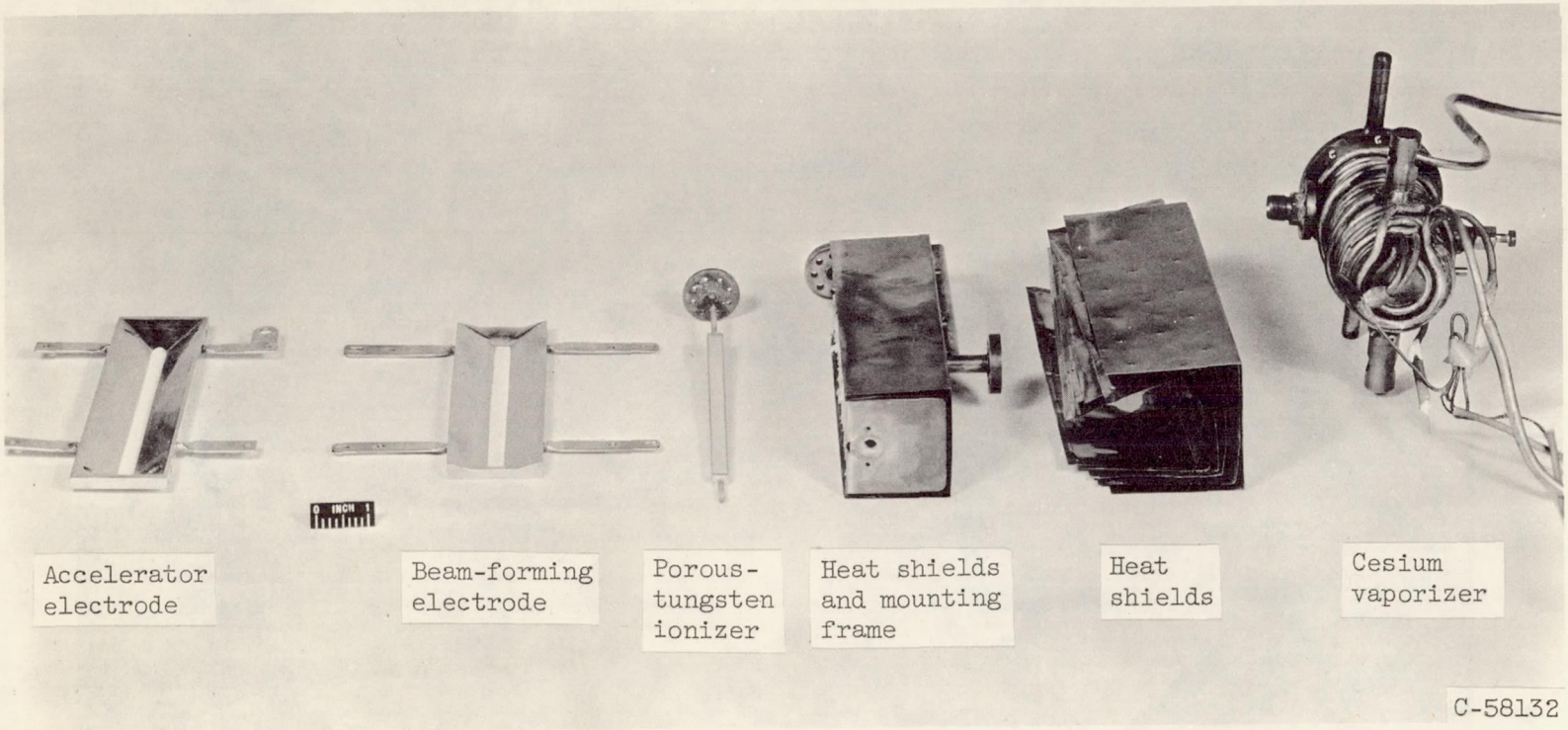

(a) Components.

Figure 3. - Ion engine.

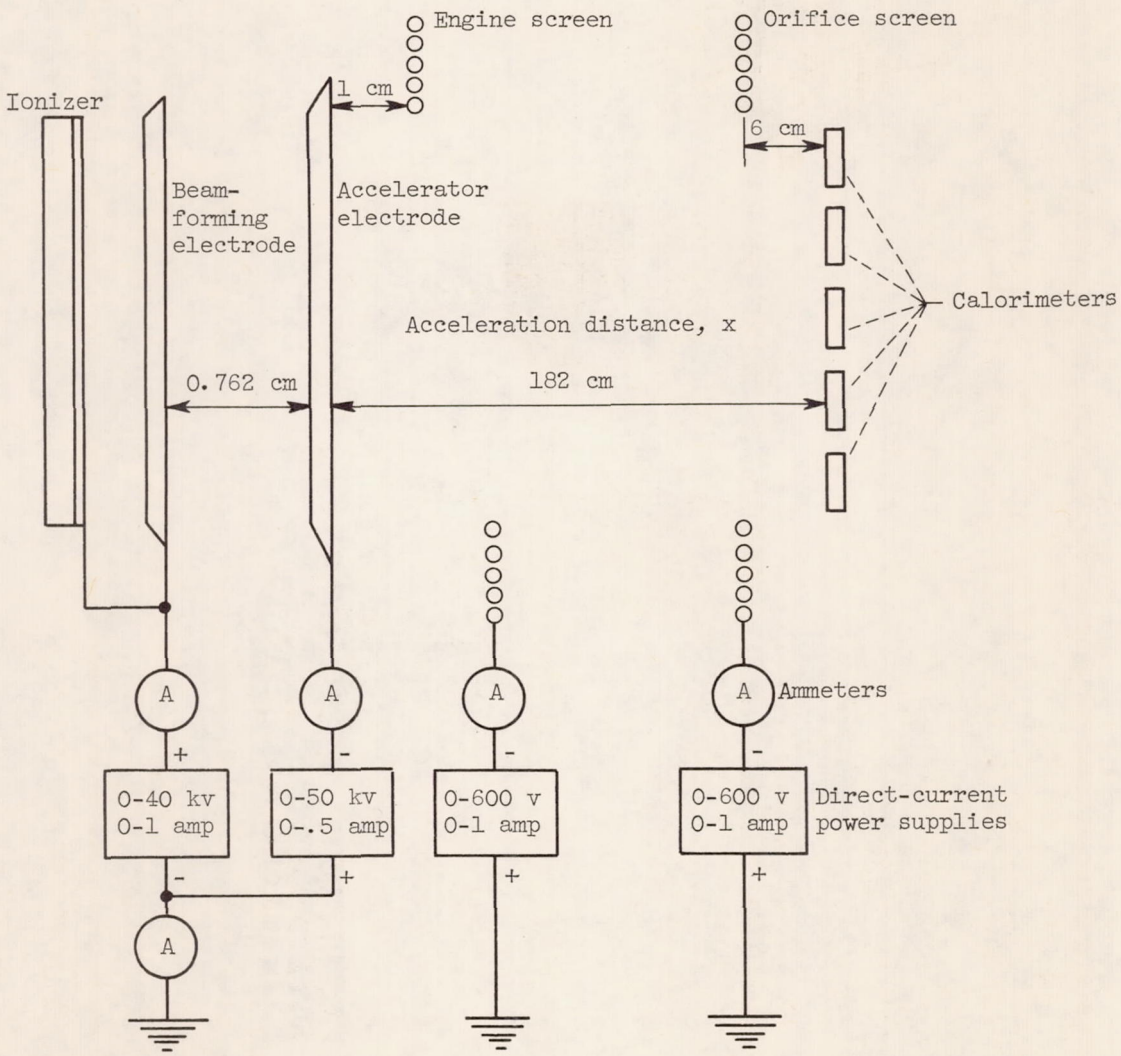

(b) Schematic of electrical system.

Figure 3. - Concluded. Ion engine.

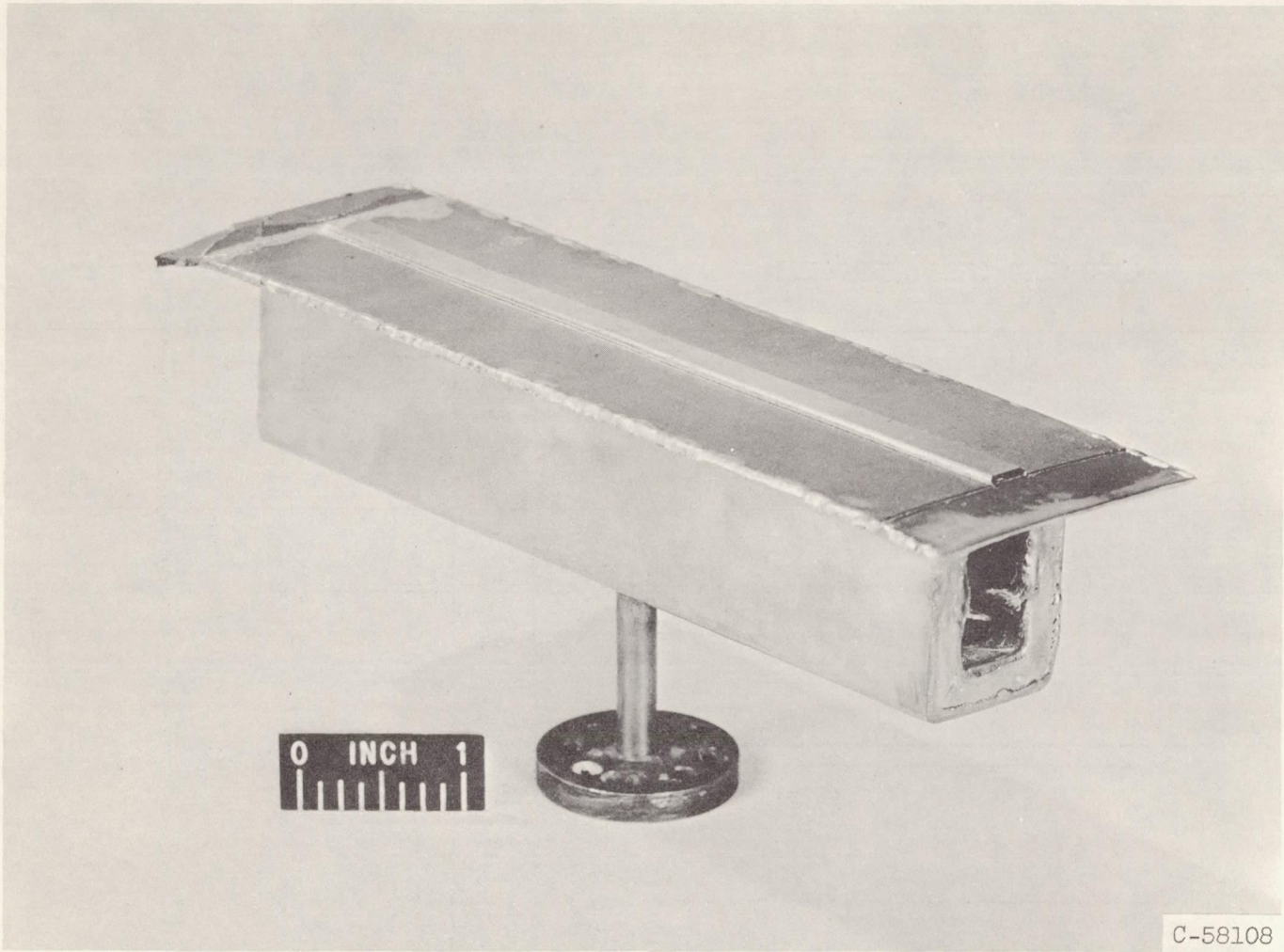

Figure 4. - First ionizer successfully constructed by means of electron-beam welding techniques.

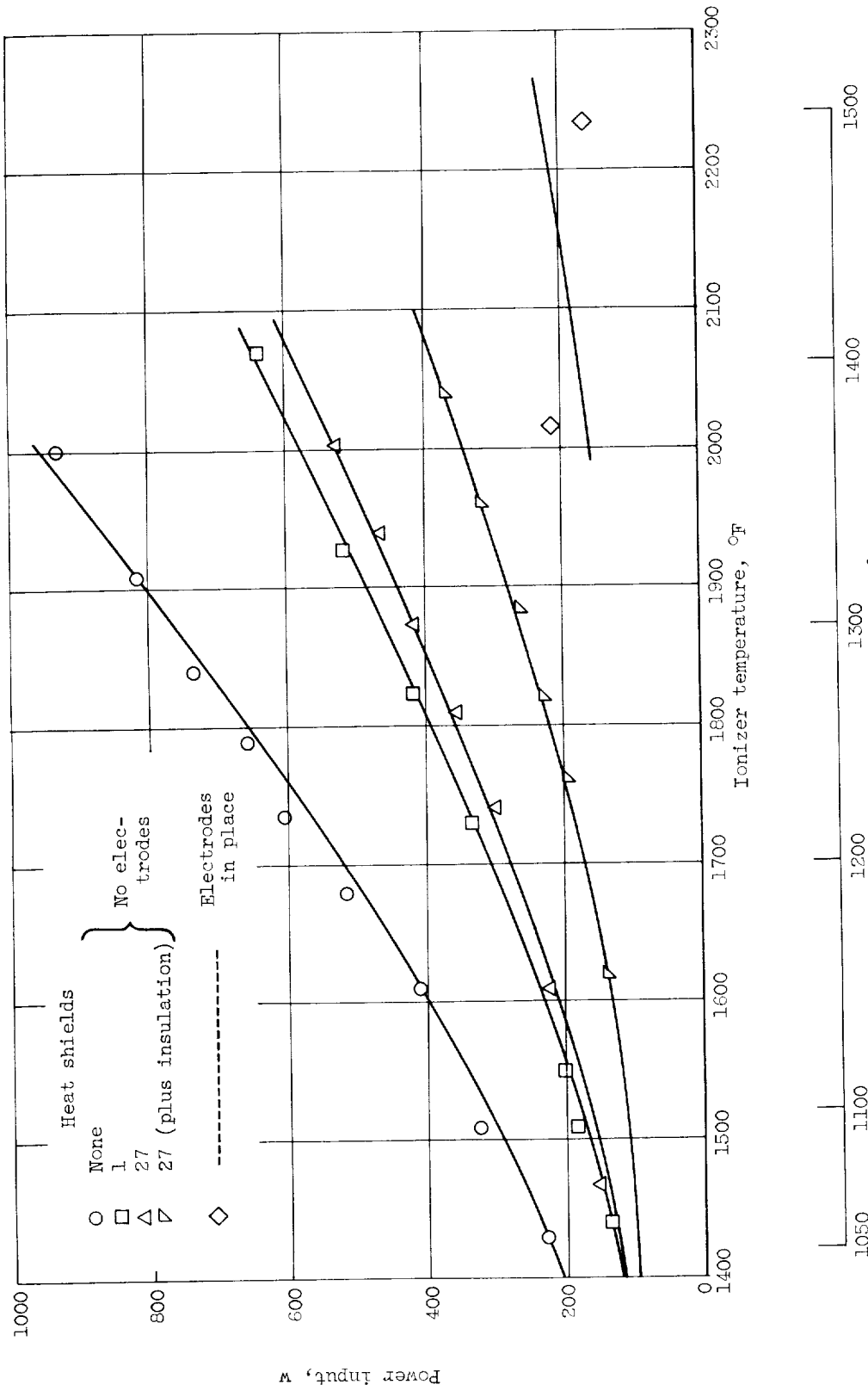

Figure 5. - Effect of heat shields for ion-emitter assembly on heater-power requirements.

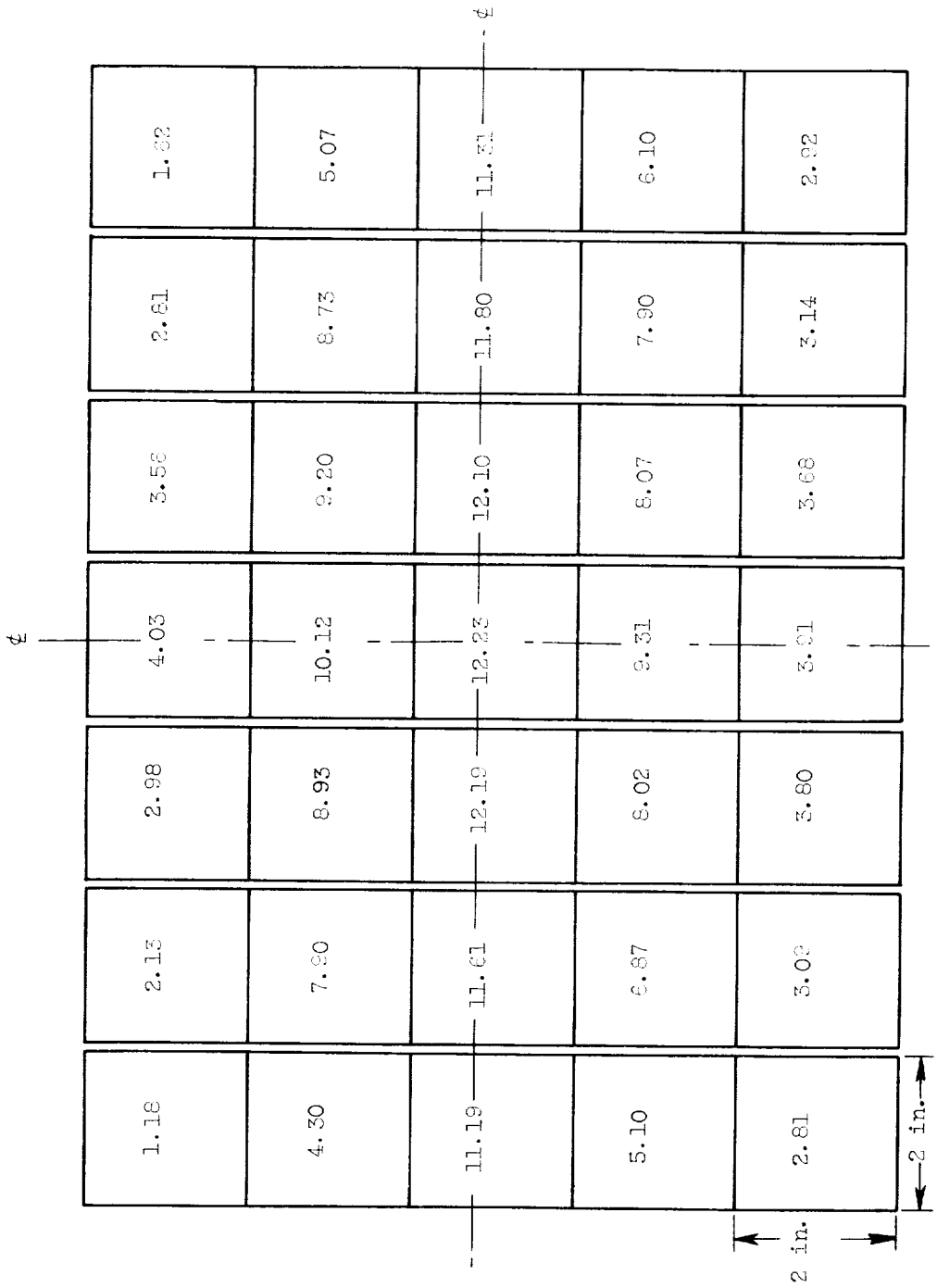

Figure 6. - Externally measured ion-beam power (in watts) total, 229.61 watts. Ion-beam current, 59 milliamperes; voltage, 5 kilovolts.

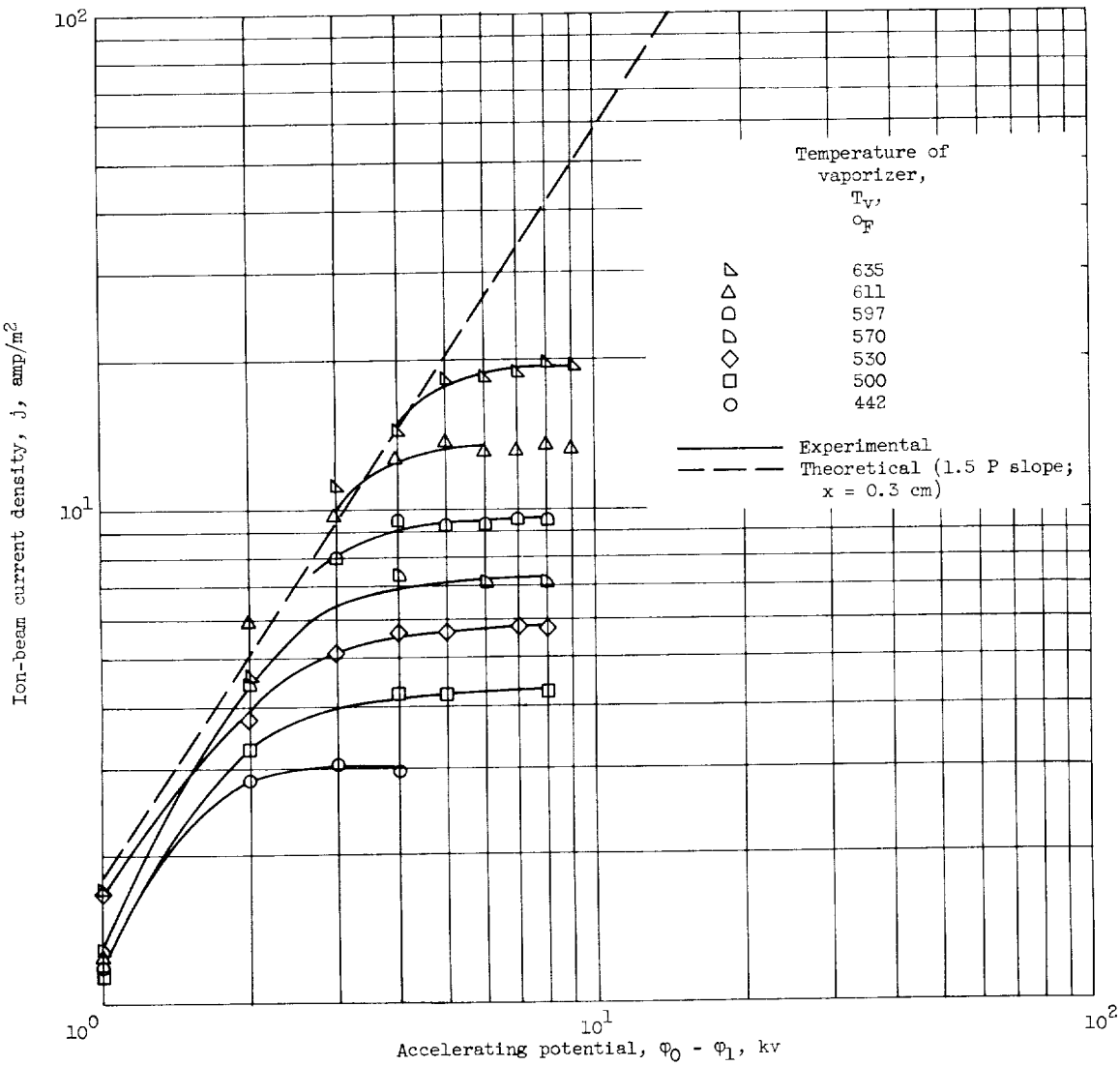

Figure 7. - Comparison of current densities obtained experimentally with those calculated from Child's Law for space-charge-limited flow as function of accelerating potential. Acceleration distance, 0.3 inch; emitter temperature, 1422^o K.

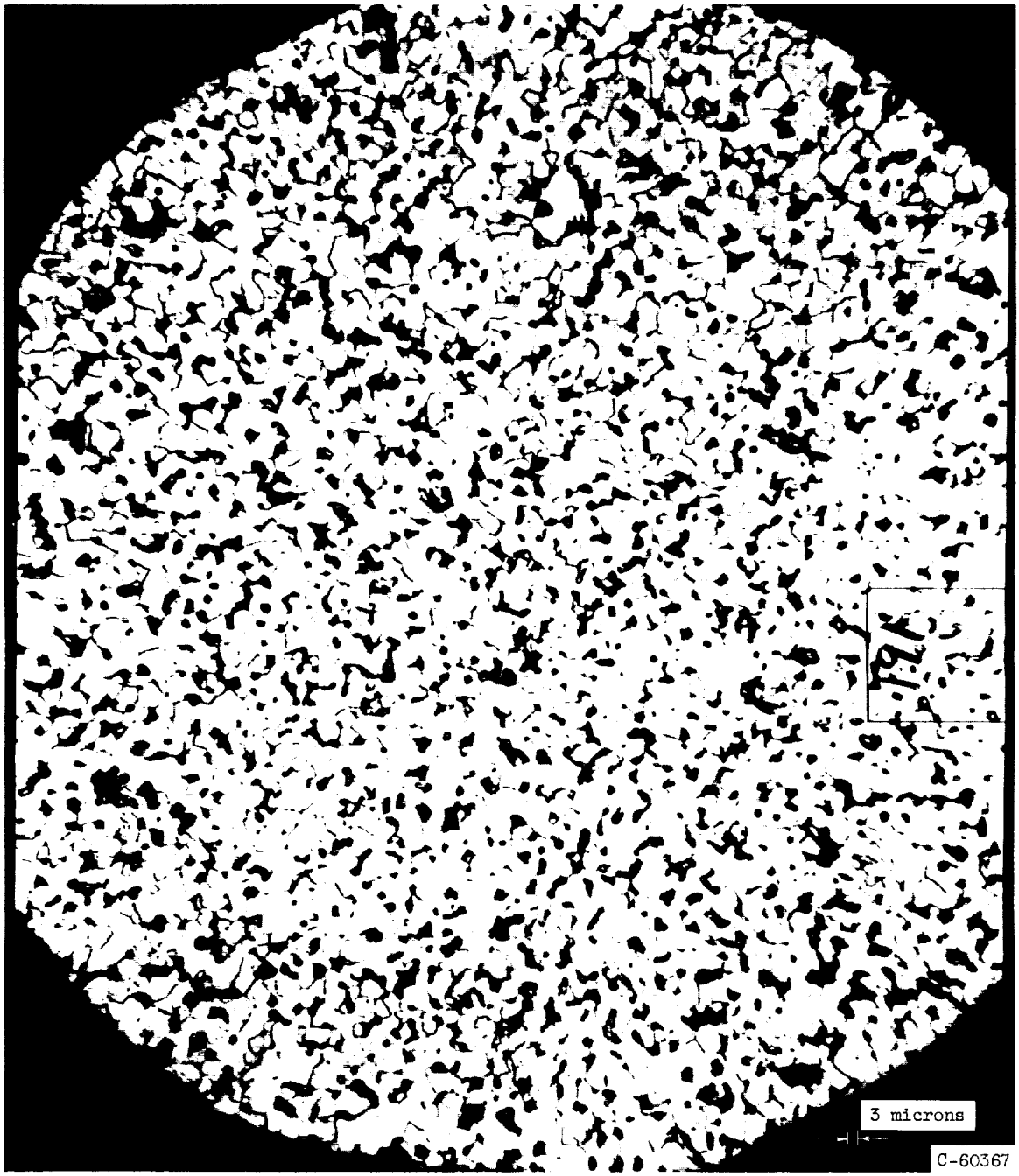

Figure 8. - Photomicrograph of porous tungsten used in this experiment. Measured average pore diameter, 2.5 to 3.0 microns.

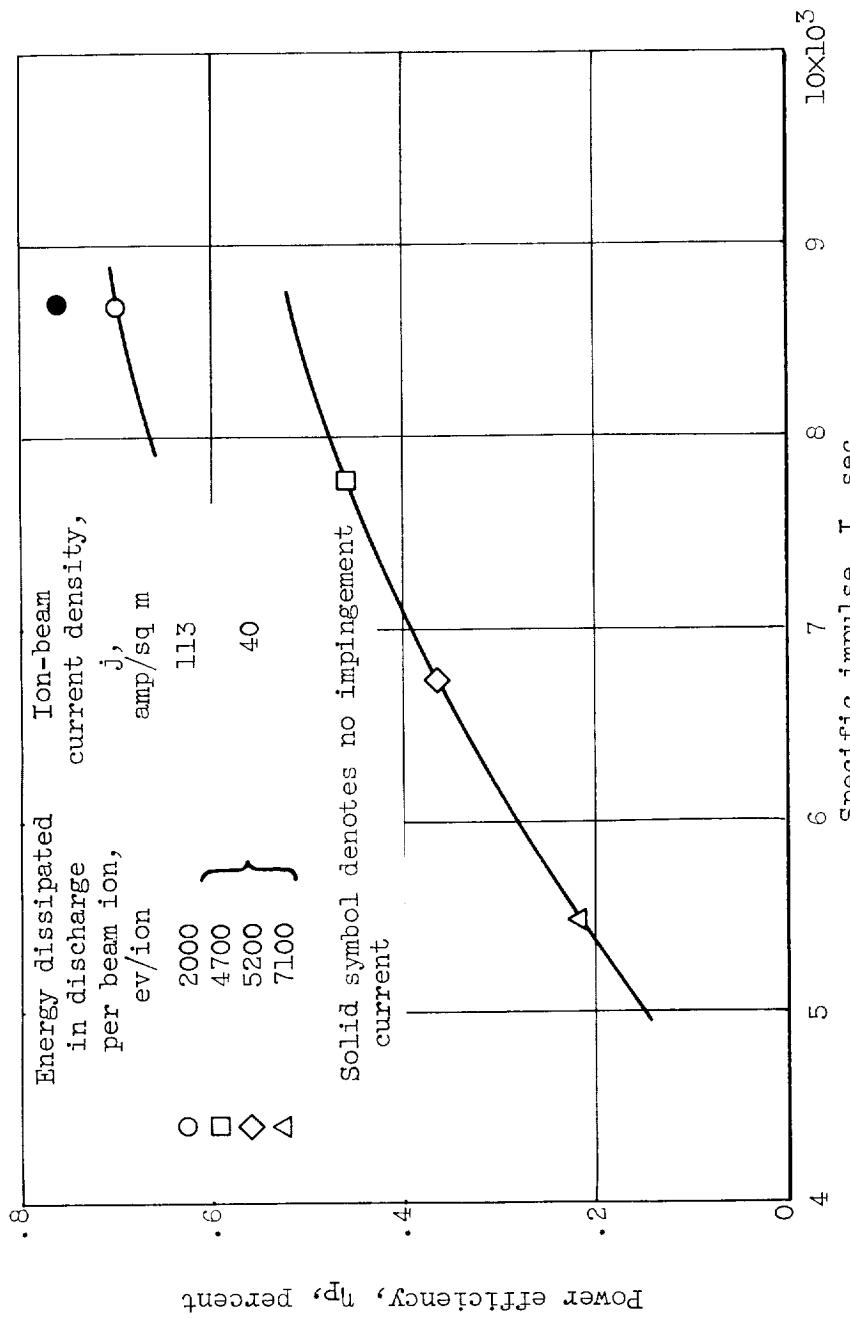

Figure 9. - Power efficiencies of porous-tungsten ionizer obtained with two current densities. Ratio of acceleration to net potential: $2\frac{1}{2}$ at specific impulse of 5500; 2 at all other specific impulses.

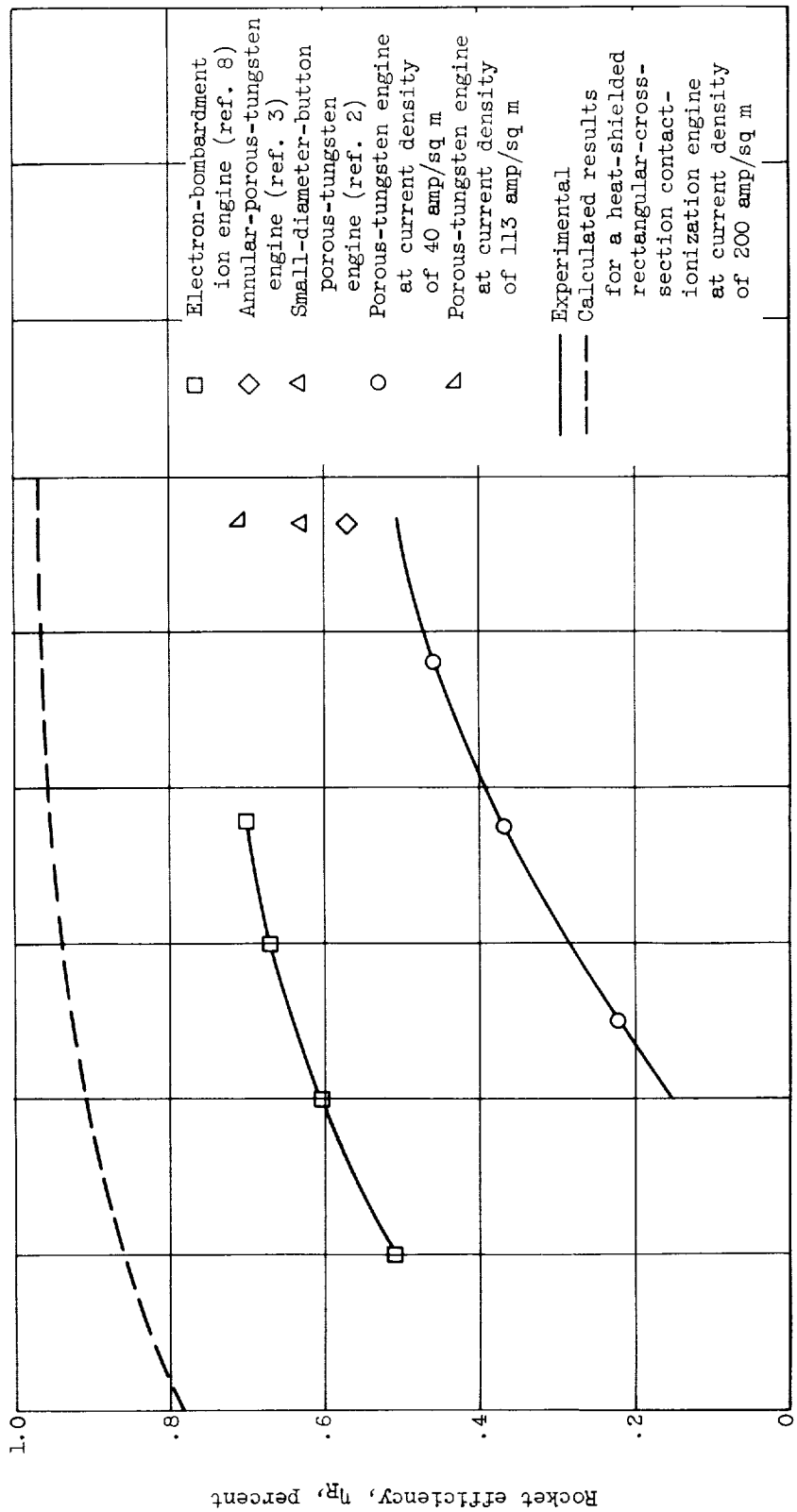

Figure 10. - Comparison of rocket power efficiencies at various effective specific impulses for various rocket engines.